Article

JOURNAL OF THE CHINESE CHEMICAL SOCIETY

Low-cost Nickel Complex Dye-sensitized Titania Nanoparticle/nanotube Composites for Solar Cells

Lirong Zhang,[a] Minh-Ngoc Ha,[b] Guanghui Sun,[b] Yuehui Fan,[b] Guanlin Zhang,[b] Yuhong Wang[b,*] and Guanzhong Lu[b]

[a]*School of Perfume and Aroma Technology, Shanghai Institute of Technology, Shanghai 201418, P. R. China*
[b]*Research Institute of Applied Catalysis, School of Chemical and Environmental Engineering, Shanghai Institute of Technology, Shanghai 201418, P. R. China*

(Received: Mar. 18, 2013; Accepted: Jul. 19, 2013; Published Online: Aug. 29, 2013; DOI: 10.1002/jccs.201300142)

In this work, high-performance dye-sensitized solar cells (DSSCs) based on new low-cost visible nickel complex dye (VisDye), TiO_2 nanoparticle/nanotube composites electrodes, carbon nanoparticles counter electrodes, and ionic liquids electrolytes have been fabricated. The electronic structure, optical spectroscopy, and electrochemical properties of the VisDye were studied. Experimental results indicate that it is beneficial to improve the electron transport and power conversion efficiency using the nickel complex VisDye and TiO_2 nanoparticle/nanotube composites. Under optimized conditions, the solar energy conversion efficiencies were measured. The short-circuit current density (J_{SC}), the open-circuit voltage (V_{OC}), the fill factor (FF), and the overall efficiency (η) of the DSSCs are 10.01 mA/cm^2, 516 mV, 0.68, and 3.52%, respectively. This study demonstrates that the combination of new VisDye with TiO_2 nanoparticle/nanotube composites electrodes and carbon nanoparticles counter electrodes provide a way to fabricate highly efficient dye-sensitized solar cells in low-cost production.

Keywords: Dye-sensitized solar cells; Nickel complexes; TiO_2 nanoparticles; TiO_2 nanotubes; Carbon nanoparticles; Ionic liquids electrolyte.

INTRODUCTION

Dye-sensitized solar cells (DSSCs) have attracted the attention of scientists all over the world because of their relatively simple fabrication, high-energy conversion efficiency and low-cost production.[1,2] For successful commercialization, it is necessary to further improve the energy conversion efficiency of DSSCs. The DSSCs are composed of the Transparent-Conducting-Oxide electrode (TCO), the metal oxide semi-conducting electrode, the dye, the electrolyte, and the counter electrode, which could be simply made by cheap materials.

Early DSSC designs involved transition metal coordinated compounds (e.g. ruthenium polypyridyl complexes) as sensitizers because of their strong visible absorption, long excitation lifetime and efficient metal-to-ligand charge transfer.[1,3] However, high cost of Ru(II) complex dye was one important factor hindering the large-scale implementation of DSSCs. Several attempts were made to replace Ru with other metals, such as Os(II), Pt(II), Re(I), Cu(I) and Fe(II).[4] In addition, the dyes used in DSSCs technology must conform to a number of essential design requirements in order to function. They must bind strongly to TiO_2 by means of an anchoring group, typically carboxylic or phosphoric acid groups, to ensure efficient electron injection into the TiO_2 conducting band and to prevent gradual leaching by the electrolyte. The LUMO of the dye must be sufficiently high in energy for efficient charge injection into the TiO_2, and the HOMO must be sufficiently low in energy for efficient regeneration of the oxidized dye by the hole-transport material. The dye must absorb solar radiation strongly with absorption bands in the visible or near-IR region, preferably covering a broad range of wavelengths. Electron transfer from the dye to the TiO_2 must also be rapid in comparison with decay to the ground state of the dye.[4]

The transition metal nickel complexes have attracted much attention due to their unique optical, electronic, magnetic, and electrochemical properties.[5-7] With these particular properties, such as superior photostability, air-stability, thermal stability, tense and broad absorption in the large spectral range extending from the UV to the near IR region, easy adjustment of the absorption range, high molecular absorption coefficient,[8] and high electron mobility,[9] many nickel complex applications have been developed. There

* Corresponding author. Tel: +86-21-60873162; Fax: +86-21-60873162; Email: yuhong_wang502@sit.edu.cn

were few reports on the application in the field of dye-sensitized solar cells.[10,11] It has been investigated as a sensitizer for DSSCs in this paper.

In DSSCs, the most important part is the nanoporous electrode made of the wide-band gap semi-conductor for supporting dye molecules and transporting photo-injected electrons. Recently researchers explored the use of ordinal TiO_2 in DSSCs, which included TiO_2 nanowires, nanorods, and TiO_2 nanotubes.[12,13] To improve electron transport, provide a large surface area to adsorb the sensitized dye, and enhance incident light harvest; the use of TNT/TNPs in DSSCs has been investigated.[14-16] The TiO_2 nanoparticle/nanotube composites were created to possess the advantages of both building blocks, high adsorbing capacities, i.e. the high surface area of nanoparticle aggregates and the rapid electron transport rate and the light scattering effect of single-crystalline nanotubes.

In this article, we report the strategic design, synthesis, and characterization of the new nickel complex sensitizer as well as its potential application in DSSCs. The TiO_2 TNP/TNT composites 9:1 (TiO_2 TNP/TNT) were prepared by mixing of containing 90 wt% TiO_2 nanoparticles and 10 wt% TiO_2 nanotubes. A novel and efficient nickel complex used as a sensitizer molecule for DSSCs with strong and broad absorptions was synthesized and the molecular structure has been calculated. The DSSCs based on combining the advantages of TiO_2 nanoparticle/nanotube composites electrodes, VisDye, ionic liquid electrolytes, and carbon nanoparticles counter electrodes have been fabricated, and the photoelectric performances were studied.

EXPERIMENTAL

Materials and chemicals. Conducting glass plate (FTO) fluoride doped tin oxide-coated glass substrate with resistance of 10 Ω/cm^2 was used as a substrate for precipitating TiO_2 porous film and was cut into 2 cm^2 (1 cm × 2 cm) sheets. All of the chemicals were from Sinopharm Chemical Reagent Co. Ltd.

Preparation of VisDye. Before addition of quinoxaline-2,3-dithiol (qdt) (201.7 mg, 1.05 mmol) in 5 mL ethanol with NaOH (84.39 mg, 2.11 mmol), $NiCl_2.6H_2O$ (243.4 mg, 1.02 mmol) in 20 mL ethanol and pyridine-3,4-dicarboxylic acid (pydc) (340.9 mg, 2.04 mmol) in 6 mL ethanol with NaOH (100 mg, 2.50 mmol) were stirred for 5 min. The resulting purple reaction mixture yielded a red/purple precipitate, filtrated and washed with ethanol. Yield = 59.8%. ^{1}H NMR (DMSO, 400 MHz)/ppm: 7.29 (s, 2H, H-qdt), 7.48 (s, 2H, H-qdt), 8.22 (m, 2H, H-pydc), 8.97 (m, 2H, H-pydc), 9.73 (m, 2H, H-pydc), 9.95 (s, 4H, H-OH). FT-IR (KBr, cm^{-1}) ν: 1615.77, 1590.23, 1488.43, 1403.30, 1167.75, 1137.60, 804.62, 750.68, 708.69, 672.88, 601.27, and 534.46. ^{13}C NMR ($CDCl_3$, 500 MHz) δ 128.35, 128.94, 141.20, 181.62.

Preparation of TiO_2 electrodes and assembly of cell. The DSSCs were constructed using TiO_2 TNP/TNT 9:1 composites (Surporting Information) containing 90 wt% TiO_2 TNP and 10 wt% TiO_2 TNT (total weight 6 g) and ground in a mortar.[14] Acetic acid (1 mL), distilled water (5 mL), and ethanol (30 mL) were added gradually drop by drop to disperse the TiO_2 TNP and TNT under continuous grinding. The TiO_2 dispersions in the mortar were transferred with an excess of ethanol (100 mL) to a tall beaker and stirred at 300 rpm. Anhydrous terpineol (10 g) and ethyl celluloses (3 g) in ethanol were added, followed by further stirring. The dispersed contents were concentrated by evaporating the ethanol in a rotary evaporator. The pastes were finished by grinding in a three-roller mill.[19] An optically transparent conducting glass (FTO, sheet resistance 10 Ω/cm^2) was washed in ethanol and deionized water in an ultrasonic bath for 10 min. The FTO glass was immersed in a 40-mm-deep $TiCl_4$ aqueous solution at 70 °C for 30 min to make good mechanical contact. A TiO_2 film with a thickness of 15 to 30 μm was deposited onto the pretreated conducting glass using the doctor-blading technique. After air-drying, the electrode was sintered at 450 °C for 30 min and cooled down to 50 °C.

Then the calcined TiO_2 electrodes was immersed in DMF solution of 3.0×10^{-3} M VisDye for 24 hr. After the substrate was adequately washed with anhydrous alcohol and dried, the dye-sensitized TiO_2 electrodes were obtained. A DSSC was assembled

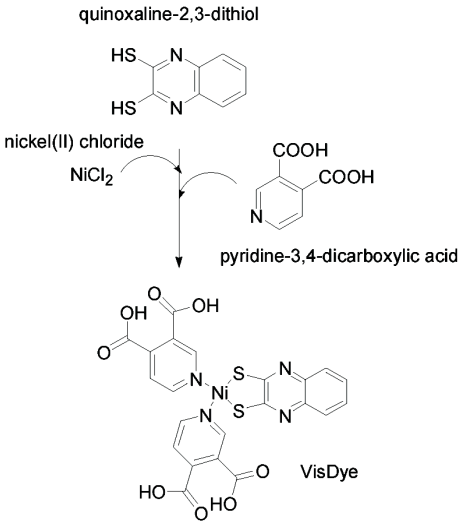

Fig. 1. Molecular structures and synthesis route for VisDye sensitizer in this research.

by filling an electrolyte solution between the dye-sensitized TiO_2 electrodes and a carbon black coated counter electrode.[20] The two electrodes were clipped together, and a cyanoacrylate adhesive was used as sealant to prevent the electrolyte solution from leaking.

Ionic liquid electrolytes: The potential of ionic liquids as solvents for DSSCs has been investigated during the last decade. The non-volatility, non-flammability, high ionic conductivity, good solvent properties and high electrochemical stability, could possess wide electrochemical potential windows of ionic liquids and make them attractive solvents in contrast to volatile organic solvents.[21] The electrolyte solution used in this work was prepared by 0.03 M I_2, 0.06 M KI, 0.6 M ionic liquid 1-Butyl-3-methylimidazolium iodide [Bmim]I, 0.6 M ionic liquid 1-Ethyl-3-methylimidazolium iodide [Emim]I in acetonitrile. Preparation of the counter electrodes (Surporting Information): Carbon black and activated carbon were used as counter electrode in this research. In order to obtain a carbon paste, 0.2 g of the carbon black powder was sequentially ground with 1 g of activated carbon, carboxy-methylcellulose (CMC) as a binder, 16 mL of distilled water, and 5 mL of ethanol. The ground carbon paste was coated on FTO glass by a doctor-blade followed by sintering for 1 hour at 150 ^{o}C in a tube furnace.

Measurement and characterization. The study of crystallinity was conducted by an X-ray diffractometer (Panalytical Xpert Pro) using Cu-Kα radiation (λ = 1.5418 Å) in angular range from 10 to 80° (2θ) at 40 mA and 40 kV. Data reduction was achieved using the MID Jade 6 program. The morphology and size distribution of all samples were determined by scanning electron microscopy SEM (Hitachi S-3400N) operated at 15 kV. FT-IR spectra of the samples as KBr discs were taken in the range of 4000–400 cm^{-1} on Nicolet-360 FT-IR spectrometer. UV-visible spectra was obtained using a Varian Cary 5000 spectrometer with a reflectance sphere in the range of 200-800 nm.

DSSC measurements: The photovoltaic test of DSSC was carried out by measuring the J-V character curves under simulated AM 1.5 solar illumination at 100 mW/cm^2 from a xenon arc lamp (XQ-500W) in the ambient atmosphere. The fill factor (FF) and the overall light-to-electrical energy conversion efficiency (η) of DSSC were calculated according to the following equations:[22]

$$FF = \frac{V_{max} \times J_{max}}{V_{OC} \times J_{SC}} \quad (1)$$

$$\eta(\%) = \frac{V_{max} \times J_{max}}{P_{in}} \times 100 = \frac{V_{OC} \times J_{SC} \times FF}{P_{in}} \times 100, \quad (2)$$

where J_{SC} is the short-circuit current density (mA/cm^2), V_{OC} is the open-circuit voltage (V), P_{in} is the incident light power, and J_{max} (mA/cm^2) and V_{max} (V) are the current density and voltage at the point of maximum power output on the J-V curves, respectively.

RESULTS AND DISCUSSION

Structural Properties of VisDye

The crystal structure of VisDye was solved by Spartan'10 and refined with CrystalMaker v2.5.1 and CrystalDiffract v1.3.2 software. The X-ray crystal structure of VisDye is shown in Fig. 2. The crystal system was triclinic with the space group of P1. The crystallographic data, conditions used for the intensity data collection and some features of the structure refinement are listed in Table 1.

The Ni atom center, two S atoms, two N atoms and one C=C are in a square-planar environment (plane Ni), which results in the p-conjugated delocalization of the seven atoms. The two Ni–S bonds and two Ni–N are approximately equal (Ni5–S2 = 2.254, Ni5–S4 = 2.250, Ni5–N9 = 2.063, Ni5–N17 = 2.051 Å) with the angles of nearly 90° for S–Ni–S, and N–Ni–N (S2–Ni5–S4 = 92.84, N9–Ni5–N17 = 89.67, N17–Ni5–S4 = 88.37, N9–Ni5–S2 =

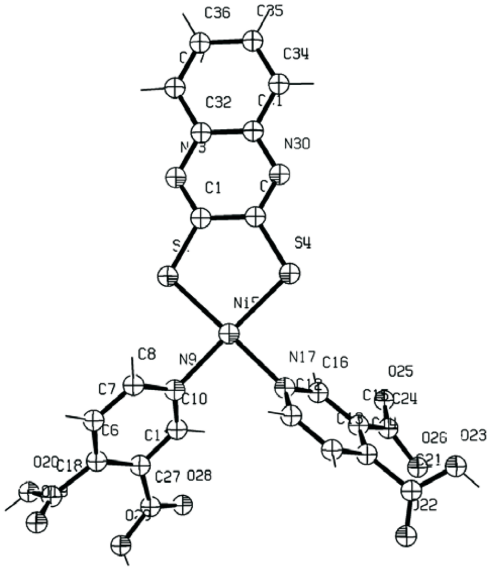

Fig. 2. ORTEP diagram of the VisDye with 50% thermal ellipsoid probability. Selected bond lengths (Å): Ni5–S2 = 2.254, Ni5–S4 = 2.250, Ni5–N9 = 2.063, Ni5–N17 = 2.051. Selected bond angles (deg): S2–Ni5–S4 = 92.84, N9–Ni5–N17 = 89.67, N17–Ni5–S4 = 88.37, N9–Ni5–S2 = 89.54, N17–Ni5–S2 = 175.81, N9–Ni5–S4 = 173.65. Selected dihedral angles (deg): S2–Ni4–N9–C10 = 123.28, S4–Ni4–N17–C12 = 107.65.

Table 1. Summary of crystallographic data for VisDye

Empirical formula	$C_{22}H_{14}N_4NiO_8S_2$
Formula weight (g/mol)	585.196
Crystal system	Triclinic
Space group symbol	P1
Lattice type	P
Unit cell lengths (Å)	a = 19.0560, b = 22.6395, c = 7.8570
Unit cell angles (deg)	$\alpha = \beta = \gamma = 90$
Unit cell volume (Å)	3389.653
Estimated density	0.2867 g/cm^3, 0.0150 atoms/Å^3
Calculated formula	C (22.00), S (2.00), Ni (1.00), N (4.00), O (8.00), H (14.00)
Covalent radius (Å)	C (0.77), S (1.04), Ni (1.35), N (0.74), O (0.66), H (0.37)
Selected bond lengths (Å)	Ni5–S2 = 2.254, Ni5–S4 = 2.250, Ni5–N9 = 2.063, Ni5–N17 = 2.051
Selected bond angles (deg)	S2–Ni5–S4 = 92.84, N9–Ni5–N17 = 89.67, N17–Ni5–S4 = 88.37, N9–Ni5–S2 = 89.54, N17–Ni5–S2 = 175.81, N9–Ni5–S4 = 173.65
Selected dihedral angles (deg)	S2-Ni4-N9-C10 = 123.28, S4-Ni4-N17-C12 = 107.65

89.54). It confirms that all the seven atoms containing the Ni center, the two S atoms, two N atoms and one C=C atoms are in the same plane. The average bond lengths for S–C and C1=C3 are 1.764 and 1.461 Å, respectively. The di-carboxylic groups are not in the same plane with the square-planar Ni–S–C ring. They make torsion angles.

Electronic Structures of VisDye

In the operation, the sunlight is absorbed by the dye molecules and excites electrons from HOMO to LUMO, which then inject into the TiO_2 electrode. These electrons percolate through the TiO_2 film and are collected by the conducting substrate. The oxidized dye molecules are regenerated by the reducing species in the electrolyte solution, predominately I^- ions.[23]

The performance of a DSSC is predominantly based on four energy levels of the component: the excited state (approximately LUMO) and the ground state (HOMO) of the photosensitizer, the Fermi level of the TiO_2 electrode,[24] which is located near the conduction-band level, and the redox potential of the mediator (I^-/I_3^-) in the electrolyte. The photocurrent obtained from a DSSC is determined by the energy difference between the HOMO (highest occupied molecular orbital) and the LUMO (lowest unoccupied molecular orbital) of the photosensitizer, analogous to the band gap, e.g. for inorganic semiconductor materials. The smaller the HOMO–LUMO energy gap, the larger the photocurrent will be due to the utilization of the long-wavelength region in the solar spectrum. The energy gap between the LUMO level and the conduction-band level of TiO_2, ΔE_1, is important, and the energy level of the LUMO must be sufficiently negative with respect to the conduction band of TiO_2 to inject electrons effectively. In addition, substantial electronic coupling between the LUMO and the conduction band of TiO_2 also leads to effective electron injection. The HOMO level of the complex must be more positive than the redox potential of the I^-/I_3^- redox mediator to accept electrons effectively (ΔE_2). The energy gaps, ΔE_1 and ΔE_2, must be larger than approximately 200 mV as driving force for each of the electron-transfer reactions to take place with optimal efficiency.[25]

In this study, density functional theory (DFT) calculations were performed with the Spartan'10 software package[26] using the B3LYP hybrid functional and the 6-31*G basis set to investigate the electronic properties of the sensitizers.[27]

Fig. 3 and Fig. 4 show the geometric and electronic

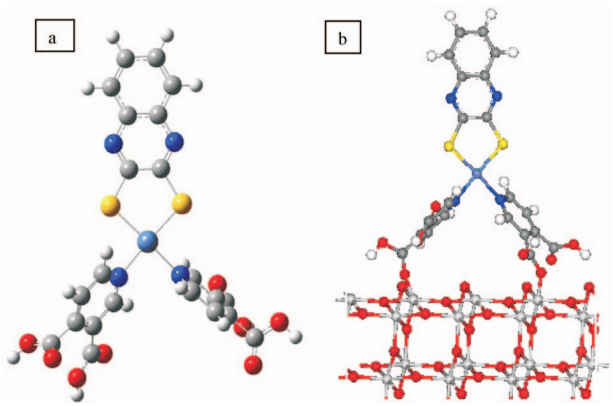

Fig. 3. Optimized geometrical structure of the VisDye (a) and VisDye/TiO_2 system in the monodentate configuration(b). Main bond distances (Å) are reported. Silver-gray) Ti, red) O, turquoise) Ni, blue) N, gray) C and yellow) S atoms.

properties of the dye performed with DFT calculations. The LUMO and HOMO energy levels (E_{LUMO} and E_{HOMO}) of VisDye are obtained in Fig. 5. The HOMO–LUMO excitation induced by light irradiation can shift the electron distribution from the middle of the molecule to the anchoring moieties, thus favoring electron injection from dye to TiO_2. The absolute energy of the HOMO is –4.95 eV, while the absolute energy of the LUMO is –2.7 eV for VisDye, respectively. The gap of HOMO and LUMO is $\Delta E_{HOMO\text{-}LUMO}$ = 2.25 eV. The fit between experimental and computational data is comparable with prior studies on transition metal complexes.[28] The calculated energies of VisDye herein are quite consistent with the experimental data (cited as D149, HOMO: –4.901 eV, LUMO: –2.873 eV).[29] For comparison, the HOMO level for N719 (calculated at the DFT level of theory in a water environment) is –5.3 eV with the LUMO at –2.7 eV.[30] The results show that the visible nickel complexes dye as a sensitizer in the DSSCs is useful and helpful for designing and modifying the structures of dyes to further improve the efficiencies of DSSCs.

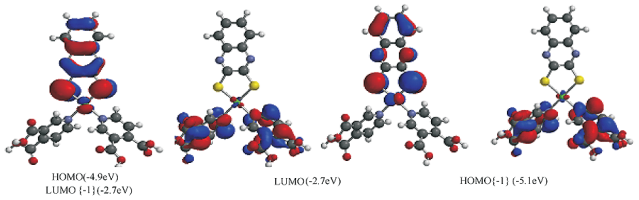

Fig. 4. Energy-level diagram and the corresponding molecular orbitals of VisDye calculated at the B3LYP/6-31G(*) basis set level of theory in a vacuum. Calculations were performed using Spartan'10 software.

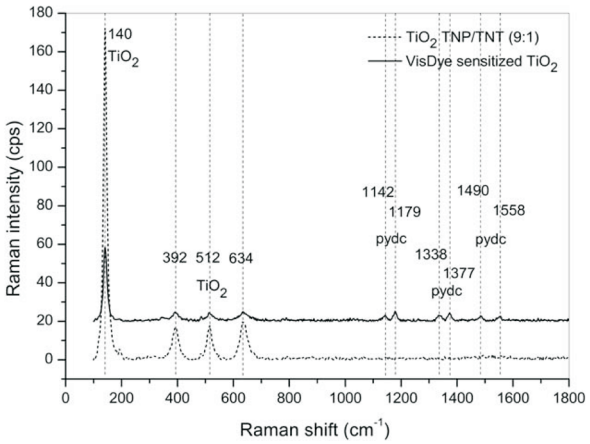

Fig. 5. Raman spectra of the TiO_2 TNP/TNT composites (9:1) and the TiO_2 TNP/TNT composites (9:1) adsorbed VisDye. Exciting line 532 nm. Laser power 5 mW. Integration time 5 min.

In general, for effective electron injection and charge separation, the electrons at LUMO should be distributed near the carboxylic group.[31] The carboxylic group is by far the most employed group for attachment of the sensitizers to the semiconductor surface. Carboxylic acid groups can form ester linkages with the surface of the metal oxide to provide a strongly bound dye and good electronic communication between the two parts.[5] The binding modes for dye sensitizers with carboxylic anchoring groups have been investigated by Galoppini and co-workers.[32] Phosphonic acids also bind strongly to metal oxides but are not frequently used. Derivates of the carboxylic acids has also been employed, such as esters and carboxylate salts.[33]

The newly synthesized VisDye with four carboxyl groups, is benefit for providing more electrons withdrawing groups and anchoring groups to nanocrystaline TiO_2.[34] The possible main binding modes of the VisDye are shown in Fig. 6. It can be seen the VisDye with more sites binding with TiO_2 can withdraw more electrons to inject the excited electron into the conduction band of TiO_2 efficiently. Furthermore, the VisDye molecular structure is also flexible; it is useful for binding with TiO_2.

As a result of the theoretical calculations, it is concluded that the HOMO–LUMO gap does not depend on the carboxyl groups,[35] but the effective anchoring on the surface of the oxide is of primary importance in the enhanced charge injection yields. With increasing the carboxyl groups in the dye sensitizers, the electron transfer efficiencies increase because of their better anchoring to the surface. During the photocatalytic reactions, the rate enhance-

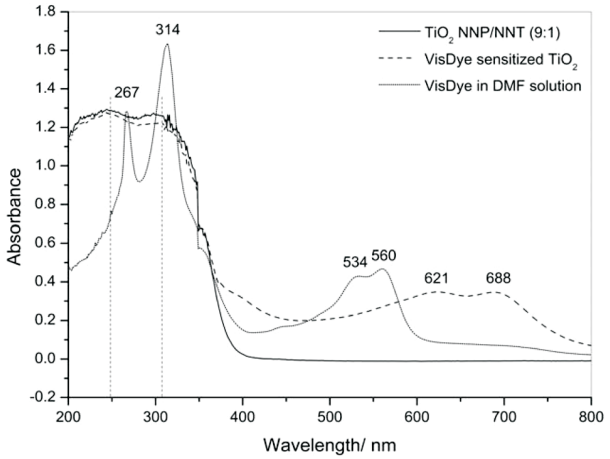

Fig. 6. UV–Vis spectra of TiO_2 TNP/TNT composites, the adsorbed VisDye sensitized on TiO_2 TNP/TNT composites layer, and VisDye in DMF solution.

ment probably lies in the fact that the dye sensitizers can be anchored on TiO_2 at more contact points therefore the electron transfer efficiencies increased.

Raman and UV-Vis Analysis of adsorbed VisDye

The TiO_2 TNP/TNT composites with and without adsorbed VisDye were analyzed by Raman spectroscopy (DXR SmartRaman Thermo SCIENTIFIC Inc., laser wavelength 532 nm) (Fig. 5). There are four peaks on the TiO_2 TNP/TNT composites curve, one intense peak at 140 cm^{-1}, and three less intense peaks at 392 cm^{-1}, 512 cm^{-1}, and 634 cm^{-1}, respectively. These results agree very well with the Raman spectra of TiO_2 anatase phase reported by Falaras et al.[36] The Raman spectra of the TiO_2 TNP/TNT composites adsorbed VisDye show the next four medium peaks at the same position of TiO_2 anatase peak, also appear six less intense peaks at 1142, 1179, 1338, 1377, 1490, and 1558 cm^{-1}. It indicates that VisDye is adsorbed on the TiO_2 surface with carboxylate COO^- bidentate coordination.

UV-Vis absorption spectra of the TiO_2 TNP/TNT composites, VisDye in DMF and adsorbed on a transparent TiO_2 TNP/TNT composites film are shown in Fig. 6. The absorption spectrum of the nickel complex VisDye adsorbed on a TiO_2 TNP/TNT composites film is expanded to the long wavelength region compared to that in DMF solution. This result can indicate the strong electronic coupling between adsorbed VisDye and TiO_2.

The absorption band of TiO_2 TNP for the tetrahedral symmetry of Ti^{4+} normally appears at approximately 250–310 nm. The maximum absorption bands in the TiO_2 TNT are slightly shifted to a shorter wavelength than that of TiO_2 TNP, but a broadened tail appears in TiO_2 TNT. Band gaps in semiconductor materials are closely related to the wavelength range absorbed, where the band gap decreases with increasing absorption wavelength.[37] The UV-Vis absorption spectrum of the VisDye in diluted DMF solution (10^{-4} mol/L) shows two distinct absorption bands. One absorption band is in the near-UV region (267-314 nm) corresponding to the π–π* electron transitions of the conjugated molecules, and the other is a wide absorption band in the visible region (500-600 nm) that can be attributed to an intramolecular charge transfer (ICT) between the donating units and the di-carboxylic acid anchoring moiety. The spectrum of TiO_2 TNP/TNT exhibites a typical optical absorption behavior of a wide-band gap semiconducting oxide, having an intense absorption band with a steep edge. When VisDye molecule is adsorbed onto the surface of the TiO_2 TNP/TNT, a new absorption band around 550-750 nm emerges in the visible region compared with that of bare TiO_2 TNP/TNT which evidently originates from the absorption of dye molecules. However, the maximum absorption at 534 nm and 560 nm of pure VisDye is shifted to 621 nm and 688 nm. The absorption peak changes might be attributed to the interaction between the dye molecules and semiconductor surface, which shows the potential application in DSSCs. The results clearly indicate that the absorption intensity of the adsorbed VisDye on the TiO_2 TNP/TNT composites layer electrode with picks is wider than the pure VisDye in diluted DMF solution. It means that the VisDye is absorbed on TiO_2 TNP/TNT composites layer electrode and changes pick position, which is ready for the enhancement of incident light harvest and improvement of light-to-electricity conversion efficiency of the DSSCs.

Electrochemical properties of adsorbed VisDye

The redox potentials of VisDye were determined by cyclic voltammetry in acetonitrile solution containing 0.03 M I_2, 0.06 M KI, 0.6 M ionic liquid 1-Butyl-3-methylimidazolium iodide [Bmim]I, 0.6 M ionic liquid 1-Ethyl-3-methylimidazolium iodide [Emim]I. All electrochemical experiments were performed using a CHI 660D electrochemical workstation (Shanghai Chen Hua Instrument Co., Ltd.) with scan condition 50 mV/s, under illumination of visible light. Cyclic voltammetry measurements were performed in a three electrode configuration using a carbon nanoparticles as a counter electrode, a Saturated Calomel Electrode (SCE) reference electrode, and one of the three types of working electrodes including a VisDye adsorption on the surface of TiO_2 TNP, TiO_2 TNT, and TiO_2 TNP/TNT composites.

Fig. 7 shows the cyclic voltammograms (CVs) of VisDye sensitized anchoring TiO_2 TNP, TiO_2 TNT and TiO_2 TNP/TNT composites electrodes. They were carried out to evaluate the electrochemical catalytic activity of the TiO_2 toward the reduction of triodide under the room conditions. In the CVs, two pairs of redox peaks are observed in all the cases. The more positive pair between 0.7 and 1.0 V is assigned to the redox reaction I_2/I_3^- and the more negative one is assigned to redox reaction I_3^-/I^-.

The TiO_2 TNP/TNT composites electrode shows larger current density than that of TiO_2 TNP and TiO_2 TNT. It indicates an improved reaction rate on the TiO_2 TNP/TNT composites, i.e. the lower charge-transfer resistance of the I_3^-/I^- redox reaction for the TiO_2 TNP/TNT composites.

Table 2. Photovoltaic performance of DSSCs based on the same VisDye and different working electrodes

Sensitizer	Working electrodes	Counter Electrode	I_{sc} (mA/cm^2)	V_{oc} (mV)	FF	η (%)
VisDye	TiO_2 TNP	Carbon nanoparticles	6.45	520	0.71	2.40
	TiO_2 TNT	Carbon nanoparticles	8.06	521	0.70	2.96
	TiO_2 TNP/TNT (9:1)	Carbon nanoparticles	10.01	516	0.68	3.52
N3[40]	TiO_2 TNP	Pt	8.9	720	0.66	4.25
	TiO_2 TNT	Pt	0.8	680	0.72	0.37
	TiO_2 TNP/TNT (Thickness ratio 7:1)	Pt	9.7	688	0.62	4.17

V_{oc}, open-circuit voltage; J_{sc}, integral photocurrent density; FF, the fill factor; η, energy conversion.

Photoelectric Performance of DSSCs

Fig. 8 shows the current-voltage photovoltaic performance curves of DSSCs based on the TiO_2 TNP, TiO_2 TNT and the TiO_2 TNP/TNT composites working electrodes at the same conditions. The open circuit voltage (V_{oc}), short-circuit photocurrent density (J_{sc}), fill factor (FF) and efficiency (η) of the DSSCs are shown in Table 2. It shows that the conversion efficiency of DSSC based on TiO_2 TNP/TNT composites is higher than that based on TiO_2 TNP and TiO_2 TNT at the same conditions.

The results are also consistent with the previous studies.[23,37,38,39] The TiO_2 TNP/TNT composites can represent a very versatile structure. The nanoparticles can provide large surface areas for the dye adsorption, while the incorporated nanotubes can enhance the light harvesting, electron transport rate, and also the mechanical properties of the films. So far, there have been limited investigations on this system. It demonstrates that the combination advantages of TiO_2 TNP and TiO_2 TNT really contributes to improve the efficiency of the energy conversion of solar cells.

The efficiency, fill factor, open-circuit voltage, and integral photocurrent for the corresponding solar cells are summarized in Table 2. It can be seen that these DSSCs have a similar V_{oc} of 0.52 V due to their same compositions. Whereas the J_{sc} is different when DSSC is based on different kind of working electrode. The best DSSC based on TiO_2 TNP/TNT are with a light-to-electric energy conversion efficiency of 3.52%, a short-circuit current density of 10.01 mA/cm^2, an open-circuit voltage of 0.516 V, and a fill factor of 68%. It indicates that the application of VisDye sensitizer in DSSCs is promising. The comparison data in Table 2 showed that the properties of VisDye were similar with literature data. However, in the most reported

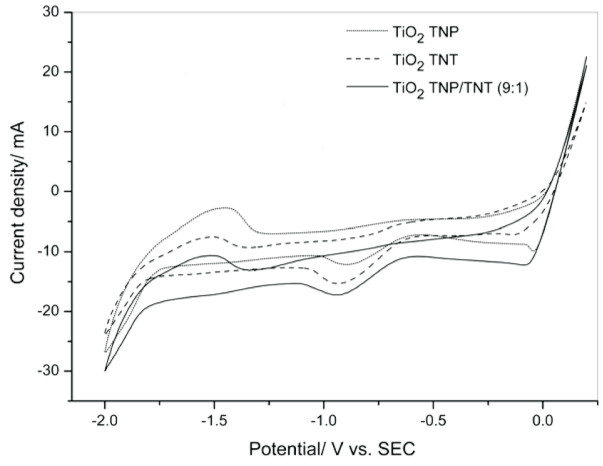

Fig. 7. Cyclic voltammograms of VisDye adsorbed TiO_2 films at a scan rate of 50 mV/s in a 0.03 M I_2, 0.06 M KI, 0.6 M ionic liquid 1-Butyl-3-methylimidazolium iodide [Bmim]I, 0.6 M ionic liquid 1-Ethyl-3-methylimidazolium iodide [Emim]I acetonitrile solution as the supporting electrolyte.

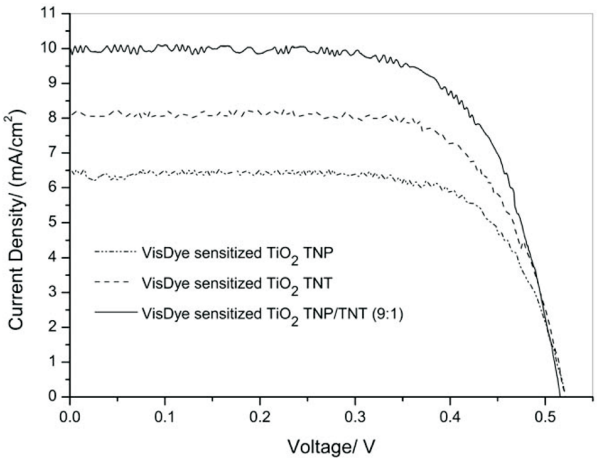

Fig. 8. Current–voltage (I–V) characteristics of the DSSC based on TiO_2 TNP/TNT composites electrode, carbon nanoparticles counter electrode, new visible nickel complex dye (VisDye), and ionic liquids electrolytes at one sun illumination (100 mW/cm, AM 1.5).

work the Pt electrode was used, the article here described the performance of carbon electrode, so the low cost was achieved in our work.

CONCLUSIONS

A new visible nickel complex dye has been designed and synthesized with conjugated linkers on the anchoring carboxylic groups. The structure, optical spectroscopy, and electrochemical properties of the VisDye were systematically studied. The results show that the VisDye are with strong and broad absorptions in the visible region and more carboxylic groups anchored on TiO_2. Therefore, the electron transfer efficiencies are increased. The DSSCs based on TiO_2 TNP/TNT and VisDye were tested. The short-circuit current density (J_{SC}), the open-circuit voltage (V_{OC}), the fill factor (FF), and the overall efficiency (η) are 10.01 mA/cm^2, 516 mV, 0.68, and 3.52%, respectively. Although the efficiencies of the fabricated DSSCs are not perfect, our results are useful and helpful for designing and modifying the structures of nickel complexes to further improving the efficiencies of DSSCs. There is also another possibility for the VisDye with the Near-IR dyes and visible dyes to be used in tandem DSSCs, hybrid DSSCs and co-sensitized DSSCs. With their particular photoelectrochemical properties, the TiO_2 TPT/TNT composites electrodes and visible nickel complex dyes will exhibit promising prospects for future application.

ACKNOWLEDGEMENTS

This work was supported by the Shanghai Municipal Natural Science Key Research Project of China (Grant No. J51503), Shanghai Municipal Natural Science Foundation of China (Grant No.11YZ221), the "Shu Guang" project supported by Shanghai Municipal Education Commission (Grant No. 10GG23) and Project supported by the National Natural Science Foundation of China (Grant No. 21273150).

REFERENCES

1. O'Regan, B.; Grätzel, M. *Nature* **1991**, *353*, 737-740.
2. Hagfeldt, A.; Boschloo, G.; Sun, L. C.; Kloo, L.; Pettersson, H. *Chem. Rev.* **2010**, *110*, 6595-6663.
3. Sepehrifard, A.; Stublla, A.; Haftchenary, S.; Chen, S. Q.; Potvin, P. G.; Morin, S. *J. New Mat. Electrochem. Systems* **2008**, *11*, 281-285.
4. Robertson, N. *Angew. Chem. Int. Ed.* **2006**, *45*, 2338-2345.
5. Paw, W.; Eisenberg, R. *Inorg. Chem.* **1997**, *36*, 2287-2293.
6. Hill, P. L.; Lee, L. Y.; Younkin, T. R.; Orth, S. D.; McElwee-White, L. *Inorg. Chem.* **1997**, *36*, 5655-5657.
7. Belo, D.; Almeida, M. *Coord. Chem. Rev.* **2010**, *254*, 1479-1492.
8. Bui, T. T.; Bonneval, B. G.; Ching, K. I. M.-C. *New J. Chem.* **2010**, *34*, 337-347.
9. Cho, J. Y.; Domercq, B.; Jones, S. C.; Yu, J. S.; Zhang, X. H.; An, Z. S.; Bishop, M.; Barlow, S.; Marder, S. R.; Kippelen, B. *J. Mater. Chem.* **2007**, *17*, 2642-2647.
10. Linfoot, C. L.; Richardson, P.; McCall, K. L.; Durrant, J. R.; Morandeira, A.; Robertson, N. *Sol. Energy* **2011**, *85*, 1195-1203.
11. Miao, Q. Q.; Gao, J. X.; Wang, Z. Q.; Yu, H.; Luo, Y.; Ma, T. L. *Inorg. Chim. Acta* **2011**, *376*, 619-627.
12. Prado, A. G. S.; Costa, L. L. *J. Hazard. Mater.* **2009**, *169*, 297-301.
13. Ratanatawanate, C.; Tao, Y.; Balkus, Jr. K. J. *J. Phys. Chem. C* **2009**, *113*, 10755-10760.
14. Lee, C. H.; Rhee, S. W.; Choi, H. W. *Nanoscale Res. Lett.* **2012**, *7*, 48-52.
15. An, H. Q.; Zhou, J.; Li, J. X.; Zhu, B. L.; Wang, S. R.; Zhang, S. M.; Wu, S. H.; Huang, W. P. *Catal. Commun.* **2009**, *11*, 175-179.
16. Huang, L. H.; Sun, C.; Liu, Y. L. *Appl. Surf. Sci.* **2007**, *253*, 7029-7035.
17. Yoo, K. S.; Choi, H.; Dionysiou, D. D. *Catal. Commun.* **2005**, *6*, 259-262.
18. Lee, C. H.; Kim, K. H.; Jang, K. U.; Park, S. J.; Choi, H. W. *Mol. Cryst. Liq. Cryst.* **2011**, *539*, 125-132.
19. Ito, S.; Chen, P.; Comte, P.; Nazeeruddin, M. K.; Liska, P.; Péchy, P.; Grätzel, M. *Prog. Photovolt. Res. Appl.* **2007**, *15*, 603-612.
20. Murakami, T. N.; Ito, S.; Wang, Q.; Nazeeruddin, M. K.; Bessho, T.; Cesar, I.; Liska, P.; Humphry-Baker, B.; Comte, P.; Péchy, P.; Grätzel, M. *J. Electrochem. Soc.* **2006**, *153*, A2255-A2261.
21. Kawano, R.; Matsui, H.; Matsuyama, C.; Sato, A.; Susan, M. A. B. H.; Tanabe, N.; Watanabe, M. *J. Photochem. Photobio. A Chem.* **2004**, *164*, 87-92.
22. Grätzel, M. *Prog. Photovolt. Res. Appl.* **2000**, *8*, 171-185.
23. Tan, B.; Wu, Y. Y. *J. Phys. Chem. B* **2006**, *110*, 15932-15938.
24. Mora-Seró, I.; Bisquert, J. *Nano Lett.* **2003**, *3*, 945-949.
25. Kalyanasundaram, K.; Grätzel, M. *Coord. Chem. Rev.* **1998**, *177*, 347-414.
26. *Wavefunction Developers:* Deppmeier, B. J.; Driessen, A. J.; Hehre, T. S.; Hehre, W. J.; Johnson, J. A.; Klunzinger, P. E.; Leonard, J. M.; Pham, I. N.; Pietro, W. J.; Yu, J. G. *Q-Chem Developers:* Shao, Y.; Fusti-Molnar, L.; Jung, Y.; Kussmann, J.; Ochsenfeld, C.; Brown, S. T.; Gilbert, A. T. B.; Slipchenko, L. V.; Levchenko, S. V.; O'Neill, D. P.; DiStasio Jr. R. A.; Lochan, R. C.; Wang, T.; Beran, G. J. O.; Besley, N. A.; Herbert, J. M.; Lin, C. Y.; Voorhis, T. V.; Chien, S. H.; Sodt, A.; Steele, R. P.; Rassolov, V. A.; Maslen, P. E.; Korambath, P. P.; Adamson, R. D.; Austin, B.; Baker, J.; Byrd, E. F. C.; Dachsel, H.; Doerksen, R. J.; Dreuw, A.; Dunietz, B. D.; Dutoi, A. D.; Furlani, T. R.; Gwaltney, S. R.; Heyden, A.;

Hirata, S.; Hsu, C.-P.; Kedziora, G.; Khalliulin, R. Z.; Klunzinger, P.; Lee, A. M.; Lee, M. S.; Liang, W.; Lotan, I.; Nair, N.; Peters, B.; Proynov, E. I.; Pieniazek, P. A.; Rhee, Y. M.; Ritchie, J.; Rosta, E.; Sherrill, C. D.; Simmonett, A. C.; Subotnik, J. E.; Woodcock III, H. L.; Zhang, W.; Bell, A. T.; Chakraborty, A. K.; Chipman, D. M.; Keil, F. J.; Warshel, A.; Hehre, W. J.; Schaefer III, H. F.; Kong, J.; Krylov, A. I.; Gill, P. M. W.; Head-Gordon, M.

27. (a) Becke, A. D. *Phys. Rev. A* **1998**, *38*, 3098-3100. (b) Lee, C.; Yang, W. T.; Parr, R. G. *Phys. Rev. B: Condens. Matter.* **1988**, *37*, 785-789.
28. McCall, K. R.; Jennings, J. R.; Wang, H. X.; Morandeira, A.; Peter, L. M.; Durrant, J. R.; Yellowlees, L. J.; Woollins, J. D.; Robertson, N. *J. Photochem. Photobiol., A* **2009**, *202*, 196-204.
29. Jose, R.; Kumar, K.; Thavasi, V.; Ramakrishna, S. *Nanotechnology* **2008**, *19*, 424004-424011.
30. Meyer, T. J.; Meyer, G. J.; Pfennig, B. W.; Schoonover, J. R.; Timpson, C. J.; Wall, J. F.; Kobusch, C.; Chen, X. H.; Peek, B. M.; Wall, C. G.; Ou, W.; Erickson, B. W.; Bignozzi, C. A. *Inorg. Chem.* **1994**, *33*, 3952-3964.
31. Nazeeruddin, M. K.; Angelis, F. D.; Fantacci, S.; Selloni, A.; Viscardi, G.; Liska, P.; Ito, S.; Takeru, B.; Grätzel, M. *J. Am. Chem. Soc.* **2005**, *127*, 16835-16847.
32. Rochford, J.; Chu, D.; Hagfeldt, A.; Galoppini, E. *J. Am. Chem. Soc.* **2007**, *129*, 4655-4665.
33. Galoppini, E. *Coord. Chem. Rev.* **2004**, *248*, 1283-1297.
34. (a) Duffy, N. W.; Dobson, K. D.; Gordon, K. C.; Robinson, B. H.; McQuillan, A. J. *Chem. Phys. Lett.* **1997**, *266*, 451-455. (b) Ramamurthy, V.; Schanze, K. S. *Photochemistry of Organic Molecules in Isotropic and Anisotropic Media (Molecular and Supramolecular Photochemistry)*; CRC Press: New York, Basel, 2003.
35. Mete, E.; Uner, D.; Çakmak, M.; Gulseren, O.; Ellialtoğlu, Ş. *J. Phys. Chem. C* **2007**, *111*, 7539-7547.
36. Falaras, P.; Goff, A. H.-L. *Sol. Energy Mater. Sol. Cells* **2000**, *64*, 167-184.
37. Kim, A. Y.; Kang, M. *J. Photochem. Photobiol., A* **2012**, *233*, 20-23.
38. Hoda H.; Zhang, L.; Li, Q. H.; Wu, J. H. *Nanotechnol. Sci. Appl.* **2010**, *3*, 45-51.
39. Yu, W. W.; Yuan, S. J.; Li, Y. G.; Zhang, Q. H.; Wang, H. Z. *ISRN Nanotechnol.* **2011**, *2011*, 1-7.
40. Xu, H.; Tao, X.; Wang, D. T.; Zheng, Y. Z.; Chen, J. F. *Electrochim. Acta* **2010**, *55*, 2280-2285.

